Selected Paper

Correlation between the *g* Tensors and the Nonplanarity of Porphyrin Rings in *Desulfovibrio vulgaris* Miyazaki F Cytochrome c_3, Studied by Single Crystal EPR

Takashi Saitoh, Yoshihiko Tachibana,[1] Yoshiki Higuchi,[2] Hiroshi Hori,[3] and Hideo Akutsu*

Institute for Protein Research, Osaka University, 3-2 Yamadaoka, Suita 565-0871

[1]Faculty of Engineering, Yokohama National University, Hodogaya-ku, Yokohama 240-8501

[2]Department of Life Science, Graduate School of Science, Himeji Institute of Technology, Kamigori-cho, Ako-gun, Hyogo 678-1297

[3]Division of Bioengineering, Graduate School of Engineering Science, Osaka University, Toyonaka 560-8531

Received August 28, 2003; E-mail: akutsu@protein.osaka-u.ac.jp

Single crystals of cytochrome c_3 from *Desulfovibrio vulgaris* Miyazaki F were examined by EPR at cryogenic temperature. The principal values and the eigenvectors are determined. The four sets of EPR signals are directly assigned to the specific four hemes in the three-dimensional structure. The relative energy levels of the three d orbitals (d_{XY}, d_{XZ}, and d_{YZ}) of each heme iron calculated from the obtained principal *g* values have shown that the energy gap between d_{XY} and d_π is small for a heme with the S_4-ruffled distortion (heme 1 and heme 2) while the energy gap is large for a heme with the S_4-saddled distortion (heme 4). The determined *g* tensor orientations indicated that the principal *g* axes of heme 1, heme 2, heme 3, and heme 4 co-rotate with the imidazole planes of the sixth ligands.

Cytochrome c_3 is an electron transport protein found in several species of sulfate-reducing bacteria. It is a small (typically $M_r \approx 14000$), soluble protein and possesses four c-type hemes per molecule. Both the fifth and the sixth ligands are histidine imidazoles for every heme. The physiological partner of this protein known so far is hydrogenase, which is assumed to be involved in the generation of the proton gradient[1] used for ATP synthesis.[2] Cytochrome c_3 has unique properties. It shows very low oxidation–reduction (redox) potentials (typically, -240 mV to -375 mV versus normal hydrogen electrode).[3] This makes it possible for the sulfate-reducing bacteria to use cytochrome c_3 as an electron transport protein under highly reduced circumstances. Furthermore, a solid film of reduced cytochrome c_3 was found to be highly electro-conductive.[4,5] The microscopic redox potentials of each heme and the interacting potentials between two hemes were determined by NMR for *Desulfovibrio vulgaris* Miyazaki F (*Dv*MF),[6,7] *Dv* Hildenborough (*Dv*H),[8,9] and *Desulfovibrio gigas* (*Dg*)[10,11] cytochrome c_3 and by electron paramagnetic spectroscopy (EPR) for *Dv*MF,[12,13] *Desulfomicrobium baculatum* Norway 4 (*Dmb*N),[14] and *Dmb* DSM1743.[15]

The magnetic properties of the iron centers of four hemes would be a factor to understand the unique properties of the redox centers. The *g* values of cytochrome c_3 are reported for *Dmb*N, *Dv*MF, *Dv*H, and *Dg*. In the case of *Dmb*N cytochrome c_3, the g_z values were assigned to each heme by single crystal EPR measurement and were correlated to the redox potential of each heme.[16] Redox titration of the EPR spectrum was carried out for the frozen *Dv*MF cytochrome c_3 and the g_z values were also correlated to the redox potential of each heme.[12,13] Magnetic susceptibility anisotropy was determined from the NMR paramagnetic shifts of *Dv*H, and *Dg* cytochrome c_3.[17] However, there is no report about the complete EPR analysis of the single crystal samples to obtain the principal tensor. The complete analysis of the single crystal is also important in view of the elucidation of the magnetic properties of the heme proteins in general. Theoretical analysis of the *g* tensor of heme irons on the basis of the crystal field theory has been extensively carried out for simple and highly symmetrical compounds.[18,19] However, the application of the theory to heme proteins raises many problems because of their reduced symmetry and complex circumstances. It has been well established in the investigations on model porphyrin complexes[20] and heme proteins[21] in the low spin state that the g_z axis is nearly parallel to the normal of a porphyrin plane. In the hemes with bis-imidazole axial ligands, the g_z value and the magnetic anisotropy are indicated to be affected by the dihedral angle between the planes of the two imidazole rings. The g_z values become larger when the dihedral angle gets closer to 90°. The spectrum of this kind of heme is called a large g_{max}-type one.[22–24] However, this theory is not enough to explain the variation of the g_z values for *Dv*MF cytochrome c_3 ($g_z = 3.38$, 2.965, 2.81, and 2.72 determined by redox titration experiments[12]), because the dihedral angle between two imidazole rings is almost parallel for the three hemes, according to the X-ray analyses.[25,26] Thus, more EPR data using single crystals are required to clarify the relation between the *g*-anisotropy and the coordination structure of the heme ligands.

Here, we report the direct determination of the principal *g* values and eigenvectors of the *g* tensor for each heme of *Dv*MF cytochrome c_3 by single crystal EPR for the first time. Furthermore, we have calculated three energy levels of the iron d orbi-

Published on the web February 10, 2004; DOI 10.1246/bcsj.77.357

tals using assigned principal g values and have examined the relationship between energy gap and porphyrin distortion. These results would provide a new insight into the role of the heme coordination in the biological functions.

Experimental

Sample Preparation. *D. vulgaris* Miyazaki F (*Dv*MF) was cultured at 37 °C, in medium C and under anaerobic conditions.[27] Cytochrome c_3 was purified as previously described.[28] The hemes are labeled as heme 1 to heme 4 in the order of sequence. Crystals of cytochrome c_3 were grown at 10 °C by the vapor diffusion method.[25] Forty to 100 μL of the protein solution, 15 mg/mL (12.5 mM Tris–HCl, pH 7.4) containing 50% (v/v) ethanol, was equilibrated against 10 mL of a buffer solution (10 mM Tris–HCl, pH 7.4) containing 60% (v/v) ethanol. Red orthorhombic crystals with space group $P2_12_12_1$ and one molecule per asymmetric unit were obtained.[25] The size of the crystal used for measurement was typically $2.0 \times 0.2 \times 0.2$ mm.

EPR Measurements. Spectra were recorded on a Varian E12 EPR spectrometer. To measure the spectra of the frozen solution, we used a 5 mW microwave at 9222 MHz with 100 kHz field modulation at 0.5 mT. The spectra were obtained at 5, 15, 30, 60, 80, and 120 K, using an Oxford ESR-900 liquid helium flow cryostat. The single crystal was mounted on a quartz sample holder so that each crystal axis (a, b, or c) is perpendicular to the magnetic field. The sample holder with the crystal was rotated manually in 10°-steps and the EPR spectrum was obtained at each step. Used for the measurement was a 10 mW microwave at 9225 MHz with 100 kHz field modulation at 1 mT. The spectra were measured at 5, 15, 50, and 80 K.

Analysis of Single Crystal EPR Spectra. The g tensors were analyzed as previously described.[21,29] The direction of the static magnetic field can be expressed as $\tilde{h} = (l, m, n)$, using the directional cosines with respect to the crystallographic axes a, b, and c. Then, the observed g factor is written as

$$g^2(l, m, n) = g_{11}{}^2l^2 + g_{22}{}^2m^2 + g_{33}{}^2n^2 + 2(g_{12}{}^2lm + g_{23}{}^2mn + g_{31}{}^2nl) \quad (1)$$

The diagonal elements and the off-diagonal elements of the g tensor can be obtained from the g values observed in the ⟨ij⟩ plane. When the static magnetic field takes the direction (l, m, 0), for example, Eq. 1 is rewritten as

$$g^2(l, m, 0) = g_{11}{}^2l^2 + g_{22}{}^2m^2 + 2g_{12}{}^2lm \quad (2)$$

Using the rotation angle φ around the 3 axis, Eq. 2 gives

$$g^2(\varphi) = g_{11}{}^2\cos^2\varphi + g_{22}{}^2\sin^2\varphi + g_{12}{}^2\sin 2\varphi = 1/2(g_{\max}{}^2 + g_{\min}{}^2) + 1/2(g_{\max}{}^2 - g_{\min}{}^2)\cos 2(\varphi - \varphi_{\max}) \quad (3)$$

where $g_{\max}$ and $g_{\min}$ are the maximum and minimum g values, respectively, and $\varphi_{\max}$ is the angle from 1 axis giving $g_{\max}$. Equation 3 shows that observed g^2 values fall on a sine curve. The values of $g_{\max}$, $g_{\min}$, and $\varphi_{\max}$ can be determined from this sine curve. Then, the elements of g tensor in the ⟨ij⟩ plane can be obtained using $g_{\max}$, $g_{\min}$, and $\varphi_{\max}$ as follows:

$$g_{ii}{}^2 = 1/2\cdot g_{\max}{}^2(1 + \cos 2\varphi_{\max}) + 1/2\cdot g_{\min}{}^2(1 - \cos 2\varphi_{\max})$$
$$g_{jj}{}^2 = 1/2\cdot g_{\max}{}^2(1 - \cos 2\varphi_{\max}) + 1/2\cdot g_{\min}{}^2(1 + \cos 2\varphi_{\max})$$
$$g_{ij}{}^2 = 1/2\cdot(g_{\max}{}^2 - g_{\min}{}^2)\sin 2\varphi_{\max} \quad (4)$$

The 3×3 matrix of g^2 tensor was made from these curves, using Eq. 4. Then, the principal values and the direction of the principal g axes were determined by diagonalizing the matrix.

Results

EPR spectra of the frozen solution of *Dv*MF cytochrome c_3 at 15 K are presented in Fig. 1. Four sets of characteristic EPR signals from the four low spin hemes are observed. The spectra show the anisotropic g values with g_z and g_x at the low- and high-field extremes and g_y in the center region. Especially, the g_x signals were separately observed, as can be seen in

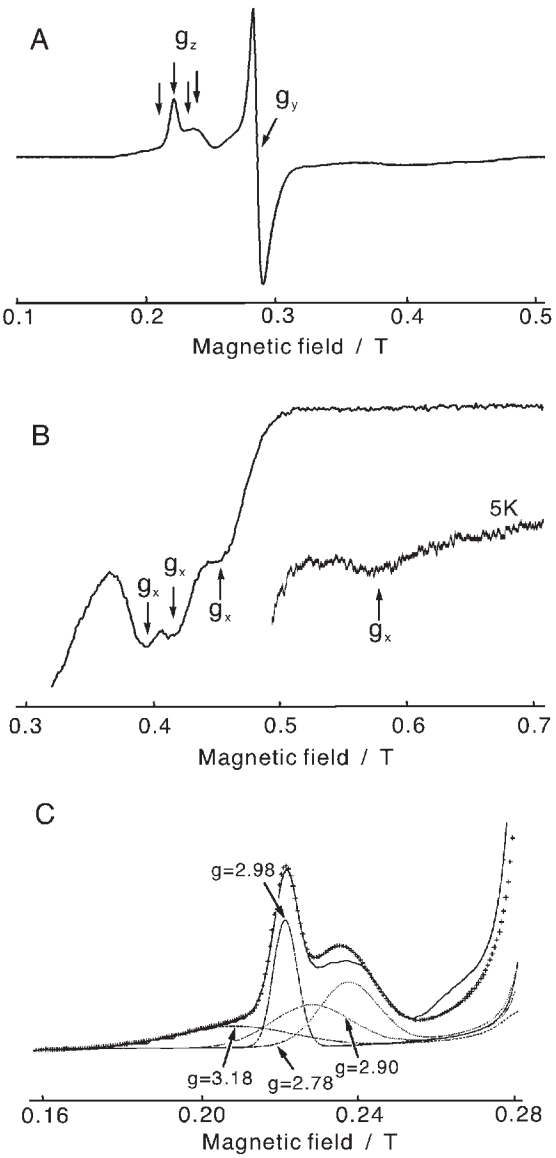

Fig. 1. EPR spectra of frozen solution of cytochrome c_3 from *Desulfovibrio vulgaris* Miyazaki F in the fully oxidized state at 15 K. A, A low field region; and B, a high field region with an inset of the spectrum at 5 K. EPR signals correspond to g_x, g_y, and g_z are indicated by arrows. C, Simulation with Gaussian line shapes in the g_z range. The used line-widths are given in Table 1. The solid and cross line indicate the observed and simulated spectra, respectively.

Table 1. The Principal g Values for Each Heme for the Frozen Solution of *Dv*MF Cytochrome c_3

	g_z	g_y	g_x
This study			
heme 1	2.98	2.31	1.43
	(6)[a)]	(4)[a)]	(30)[a)]
heme 2	3.18	2.29	1.15
	(30)[a)]	(10)[a)]	(50)[a)]
heme 3	2.90	2.30	1.57
	(20)[a)]	(5)[a)]	(25)[a)]
heme 4	2.78	2.30	1.69
	(15)[a)]	(5)[a)]	(30)[a)]
Redox titration[b)]			
heme 1	2.97	—	1.425
heme 2	3.29	—	—
heme 3	2.93	—	1.59
	2.81		
heme 4	2.75	—	1.675
Reported by Salgueiro et al.[c)]			
heme 1	−2.97	2.31	−1.59
heme 2	−3.29	2.31	—
heme 3	−2.81	2.31	−1.675
heme 4	−2.903	2.31	−1.425

a) Line-widths used for the simulation in mT. b) Ref. 12, 13. c) Ref. 30.

Fig. 1B. The analysis of the g_z region by the simulation with Gaussian line shapes gave the best fit with $g_z = 3.18$, 2.97, 2.90, and 2.78 (Fig. 1C). When temperature was increased, the signals corresponding to $g_z = 3.18$ and $g_x = 1.15$ disappeared at 30 K. Thus, this set of g_z and g_x should originate from the same heme. On the basis of these observations, four sets of g_x, g_y, and g_z were fitted to the observed spectrum by the simulation with Gaussian line shapes. The best-fit values are given in Table 1 together with their line-widths. In this study, we could observe the g_x signal at 1.15 that had not been observed in the previous studies. This was attributed to heme 2.

The EPR signal of cytochrome c_3 crystal was measured at 15 K by rotating the crystal around the crystal axes, a, b, and c, respectively. The respective signals were labeled as g1, g2, g3, and g4 in the order of the g_z value: from large to small. The g^2 values in the ⟨ab⟩, ⟨ac⟩, and ⟨bc⟩ planes are presented as functions of φ in Figures 2A, B, and C, respectively. Two symmetric curves with respect to each crystal axis were observed, because this crystal has $P2_12_12_1$ symmetry and one molecule per asymmetric unit. The maximal error among the crystal planes was 9.9°; this came from the uncertainty of g values that originated from the line width of the signals and from the uncertainty of mounting the crystal on the sample holder. Two sets of the principal g tensors and eigenvectors were obtained, because of the signs of the off-diagonal elements. The set significantly different from the values for the frozen solution was discarded. The obtained principal g values were assigned to specific hemes by comparing the direction of principal g_z axis with those of heme normals obtained by X-ray crystallographic analysis. The heme normal was defined as the vector perpendicular to the plane formed by pyrrole N_1–N_3 and N_2–N_4 vectors. The directions of the principal g_z axis and those of the heme

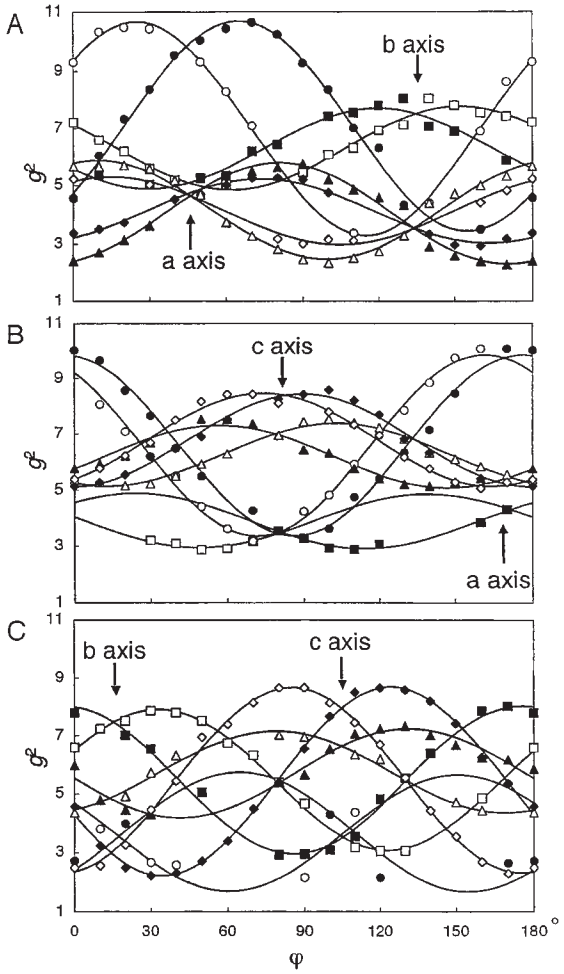

Fig. 2. Rotational angle (φ) dependence of g^2 obtained from single crystal EPR measurement at 15 K. Circles, diamonds, squares, and triangles represent g1, g2, g3, and g4 signals, respectively. A, In the ⟨ab⟩ plane; B, in the ⟨ac⟩ plane; and C, in the ⟨bc⟩ plane. The crystal axes a, b, and c are indicated by arrows. Solid lines are simulated curves using the g values in Table 2.

normal are presented in an equatorial stereographic projection on the ⟨ab⟩ plane (Fig. 3A). In this presentation, each direction is defined by the polar angles, θ and ϕ, in the crystal coordinates (Fig. 3C). The directions of principal g_z axis of g1 and g3 almost coincide with the heme normals for heme 2 and heme 3, respectively. Since these g_z directions are relatively separated from the others, g1 and g3 can be unambiguously assigned to heme 2 and heme 3, respectively. The EPR signal of heme 2 is expected to be the large g_{max} type ($g_z > 3.0$), because the dihedral angle between two imidazole ligands ($\beta = 64°$) is larger than 45°.[18] In fact, the g_z value of heme 2 (3.26) was the largest among those of four hemes, which supports our assignment. The directions of the normals of heme 1 and heme 4 are close to each other. To make a clear assignment, we present another equatorial stereographic projection on the ⟨ac⟩ plane in Fig. 3B. It shows that g2 and g4 can be assigned to heme 1 and heme 4, respectively. The signal of g2 corresponding to $g_z = 2.98$ was very sharp near the c axis on the ⟨ac⟩ and ⟨bc⟩ planes. Since the heme 1 normal is close to the c axis, this phenomenon supports

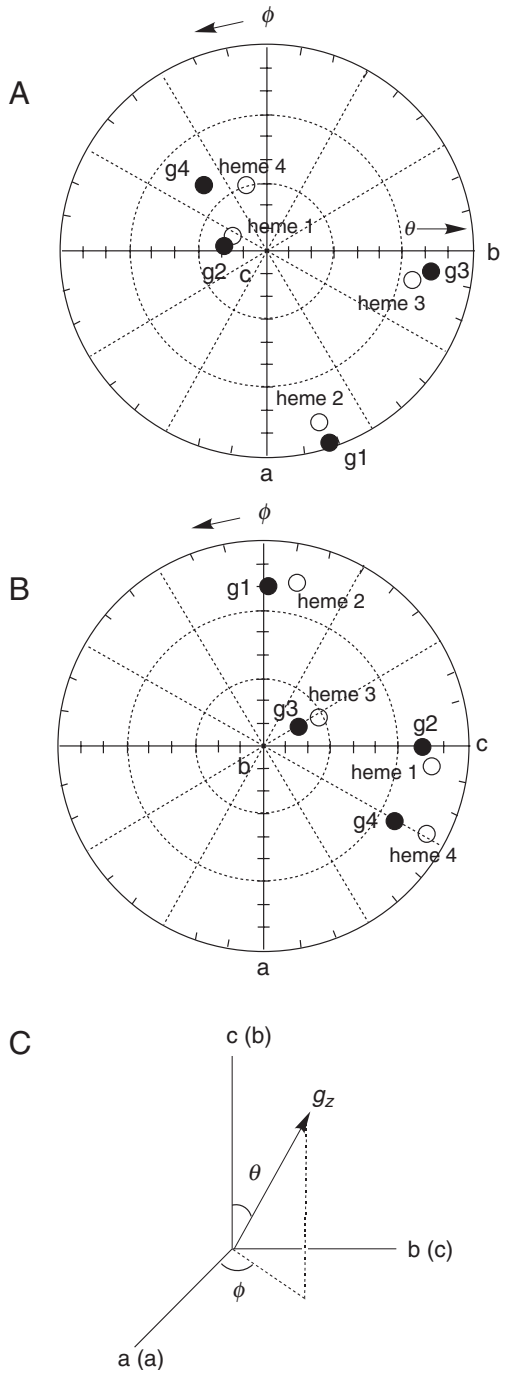

Fig. 3. Stereogram of the directions of the g_z axes and of the heme normals in the crystal coordinate (a,b,c). The closed and open circles stand for the directions of the g_z axis and the heme normal, respectively. A, The ⟨ab⟩ plane; and B, the ⟨ac⟩ plane. C, The definition of θ and ϕ.

our assignment. The obtained principal g values and the eigenvector of the principal g_z axes are summarized in Table 2. The principal g values obtained from the single crystal are essentially same as the g values obtained from the frozen solution within the experimental errors. The g values for the frozen solution reported earlier are also shown in Table 1 for comparison. Our data are in good agreement with those obtained by redox titration,[12,13] but are different from those estimated by Salgueiro et al.[30] The latter group used the data reported by the former group. Nevertheless, the assignment of g_z values for heme 3 and heme 4 are opposite and the assignment of g_x values are completely different. Since their assignments of the g values were based on indirect analysis, the reliability of the assignment would be low in comparison with there liability of assignments by redox titration. Furthermore, one g_x was missing in the original data. In contrast, our result was deduced from the direct and complete analysis of the crystal.

Discussion

The Crystal Field and Spin Orbit Coupling. Taylor has developed a crystal field theory on the g tensor of a low spin d^5 system using one-hole formalism.[31] For iron(III) heme proteins and porphyrin complexes, the spin orbital and crystal field energies are comparable in magnitude and are much larger than typical Zeeman energies. On the basis of this theory, the crystal field, spin orbital energies, and their wave functions can be calculated form the g values. The tetragonal splitting (V/λ), the energy gap of d_{XZ} and d_{YZ}, and the rhombic splitting (Δ/λ), the energy gap of d_{XY} and d_π (d_{XZ} and d_{YZ}) are given as follows:

$$V/\lambda = g_x/(g_z + g_y) + g_y/(g_z - g_x) \quad (5)$$

$$\Delta/\lambda = g_x/(g_z + g_y) + g_z/(g_y - g_x) - (V/\lambda)/2 \quad (6)$$

Here, the coordinates (X, Y, Z) and (x, y, z) are defined as the principal frames for the wave functions and the g tensors, respectively. They are not the same, in general.

The energy gaps among d_{XZ}, d_{YZ}, and d_{XY} orbitals of each heme were calculated from Eqs. 5 and 6, using the g values in Table 2. The results are schematically presented in Fig. 4. The positive sign of Δ/λ for every heme indicates that the energy level of d_{XY} is lower than those of d_{XZ} and d_{YZ}. In previous studies on heme proteins and model porphyrin complexes, it has been reported that the V/λ and Δ/λ values correlate with the dihedral angle between the imidazole planes of the fifth and sixth ligands. Namely, V/λ and Δ/λ become smaller when the dihedral angle gets closer to perpendicular.[22–24] In *Dv*MF cytochrome c_3, the dihedral angle between the imidazole planes is 64° for heme 2 and close to 0° (Fig. 4) for the others.[25] Actually, V/λ and Δ/λ of heme 2 are smaller than the others, in good agreement with the prediction. However, V/λ and Δ/λ of heme 1, heme 3, and heme 4 also show the variations in spite of their similar dihedral angles. A possible explanation for this is the difference in porphyrin structure. The correlation between nonplanarity of porphyrin ring and redox potentials has been studied by resonance Raman, molecular mechanics, and normal coordinate analysis for several cytochromes c_3.[32] In the case of *Dv*MF cytochrome c_3 crystal, heme 1 and heme 2 take on S_4-ruffled type (see Fig. 5B) distortions, while heme 4 takes on a S_4-saddled type (see Fig. 5B) distortion. Heme 3 is almost planner. Heme 1 is unusual in the light of the known ligand orientation. In most porphyrin complexes with S_4-ruffled distortion, two axial ligands are perpendicular to each other because of the steric hindrance between ligands and porphyrin.[33–35] This could be the reason of the asymmetry in the axial Fe–N coordination bonds (0.188 nm for the fifth and 0.202 nm for the sixth).[25] This would be realized only in the presence of a

Table 2. The Principal g Values and Directions of the Principal g_z Axes in the Single Crystal of *Dv*MF Cytochrome c_3

	g_z	g_y	g_x	g_z angle to axis[a)]			Angle between g_z and heme normal
				a	b	c	
heme 1	2.98	2.31	1.47	−89°	−71°	20°	7°
heme 2	3.26	2.33	1.13	19°	71°	89°	10°
heme 3	2.84	2.28	1.57	82°	19°	73°	9°
heme 4	2.81	2.29	1.70	−30°	−31°	40°	18°

a) The axes a, b, and c are defined in the crystal coordinate.

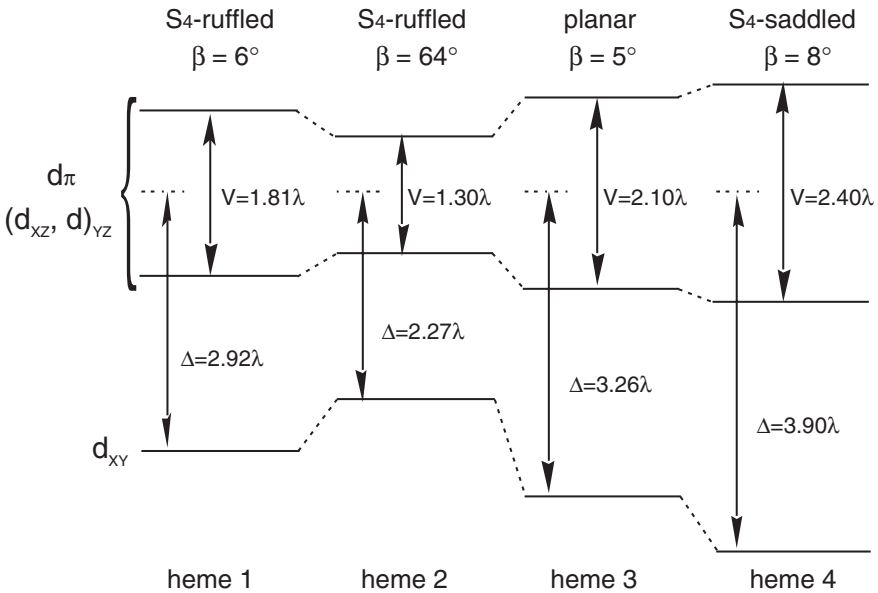

Fig. 4. Energy diagrams of the d_{XY} and d_π orbitals of each heme. V and Δ are the rhombic and tetragonal splittings, respectively. λ is the spin orbit coupling constant (approximate 280 cm^{-1} for ferric hemes[17]). The energy level of the d_π orbitals tentatively placed at the constant position. The distortion type of the porphyrin is shown on the top. The β is the dihedral angle between two axial ligand planes.

polypeptide chain around the heme. Interestingly, the linewidth of the heme 1 signal is the narrowest among those of four hemes.

It is reported for model porphyrin complexes that, when the porphyrin plane is distorted to the S_4-ruffled form like heme 1 and heme 2, the d_{XY} orbital is destabilized because of increasing the interaction between the d_{XY} and porphyrin a_{2u} orbitals, and the d_π (d_{XZ} and d_{YZ}) orbitals are stabilized because of decreasing the interactions between the d_π and porphyrin $3e_g$ orbitals.[36,37] This would be also the case with heme 1 and heme 2 of *Dv*MF cytochrome c_3. Furthermore, the central irons of heme 1 and heme 2 deviate from the porphyrin plane (heme 1 = 0.11 Å heme 2 = 0.07 Å) and pyrrole nitrogen plane (heme 1 = 0.05 Å heme 2 = 0.06 Å), while Fe is positioned in the center of porphyrin plane in heme 3 and heme 4.[25] In contrast to the S_4-ruffled form, the d_{XY} orbital of the S_4-saddled form is stabilized because of decreasing the interaction between d_{XY} orbital and porphyrin a_{2u} orbital, and its d_π orbitals are destabilized because of increasing the interaction among the d_π orbitals and porphyrin $3e_g$ orbital.[38] Thus, the distortions of the porphyrin planes of *Dv*MF cytochrome c_3 can explain the variation of the energy diagrams in Fig. 4. Consequently, the change of the energy diagram of each heme in Fig. 4 can be ascribed at least partly to the distortion of the porphyrin plane.

Peisach et al. classified porphyrins coordinated with bis-imidazoles to groups B and H using Δ/λ and V/λ.[39] Groups B was assigned to the porphyrin with protonated imidazoles. In the case of group H, one or both ligands are assumed to be imidazolate rather than imidazole. In the case of *Dv*MF cytochrome c_3, heme 4 falls in group H, while heme 1 and heme 3 are on the border of groups B and H. Heme 2 is close to group B. This analysis suggests that some of the imidazoles coordinated to the four hemes in cytochrome c_3 have the nature of imidazolate to some extent. This can be one of the reasons that cause the extremely low redox potentials of cytochrome c_3.

The Orientation of the Principal *g* Tensors. The orientation of the principal g axes determined by single crystal EPR analysis are illustrated in Fig. 5, together with two histidine ligands for each heme. The orientation of the principal coordinate with respect to the heme plane could not be decided because of the crystal symmetry. Thus, the g_z axes can be either up or down. The principal g_z axes of heme 1, heme 2, and heme 3 tilt from the heme normal to C_6 by 7°, from that normal to N_3 by 10°, and from that normal to C_5 by 9°, respectively. On the other hand, the principal g_z axis of heme 4 tilts by 18° to N_1 with the g_y and g_x axes shifting from the heme plane by 9°

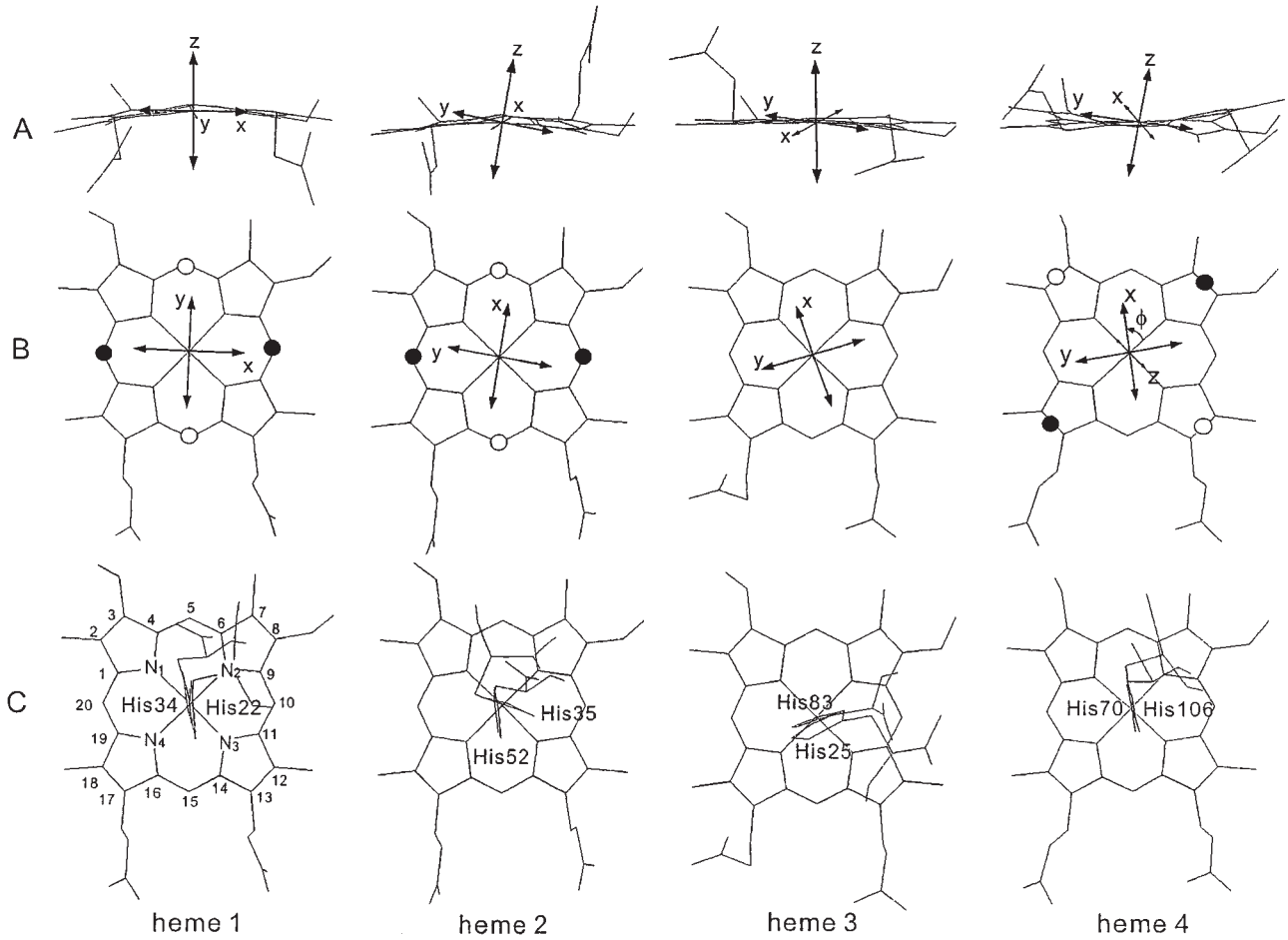

Fig. 5. Orientation of the principal g axes and the coordinated imidazole planes for each heme. The labels x, y, and z stand for the directions of principal g_x, g_y, and g_z axes, respectively. A, Views from the propionate group side. B and C, Views from the sixth ligand. In B, the g_z axes of heme 1, heme 2, and heme 3 are not shown because they almost overlap with the origin. Heme 1 and heme 2 are distorted in the S_4-raffled type and heme 4 is distorted in the S_4-saddled type. The open and closed circles represent the deviation of the atoms upward and downward from the prophyrin plane, respectively. The numbering of the heme atoms is given in C.

and 15°, respectively. The deviation of the g_z axis from the heme normal was also reported for heme 4 of *Dmb*N cytochrome c_3 (19.5°).[16] Crystal structures of cytochrome c_3 from *Dv*MF[25] and *Dmb*N[40] showed that the general architecture of the four hemes is essentially the same. The principal coordinate of heme 4 of both cytochromes c_3 might be affected by the location close to the carboxyl terminus of the protein.

The correlation between orientation of the principal axes of the g tensor and the axial ligands has been investigated using hemoproteins and Fe–porphyrin model complexes. The counter-rotation of the g_x axis with respect to the rotation of axial ligand planes was mentioned by Turner using the NMR data.[41–43] Shokhirev et al. have extensively investigated the co- and counter-rotations of the g tensor and ligands on the basis of crystal field theory.[18] Their results suggested that there is a correlation between the rotations of the g tensor and the sixth ligand, although they did not give any decisive comments. Turner et al., however, claimed that the average angle of ligand planes is relevant to the rotation of the g tensor using the magnetic susceptibilities determined by NMR.[17] Bertini et al. introduced the dihedral angle between the ligand planes in addition to the average angle.[44] The angles from the N_2–Fe–N_4 axis to

Table 3. The Angles of Principal g Axes and Coordinated Imidazole Rings with Respect to the N_2–Fe–N_4 Axis

	g_x axis	g_y axis	Imidazole plane[a)]
heme 1	−49°	41°	50° (His 22[b)])
			55° (His 34[c)])
heme 2	35°	−55°	−63° (His 35[b)])
			53° (His 52[c)])
heme 3	65°	−25°	−19° (His 25[b)])
			−27° (His 83[c)])
heme 4	56°	−34°	52° (His 70[b)])
			58° (His 106[c)])

a) Ref. 25. b) The sixth ligand. c) The fifth ligand.

principal g axes and to coordinated imidazole rings in this study is shown in Table 3. In the case of *Dv*MF cytochrome c_3 crystal, the g_x axis of heme 1 rotates −49° (clockwise) from the N_2–Fe–N_4 axis, while His 22 (sixth ligand) and His 34 (fifth ligand) rotate 50° and 55°, respectively, in good agreement with the counter-rotation theory. However, the g_x axis of heme 4 rotates 56°, while His 70 (sixth ligand) and His 106 (fifth ligand) rotate 52° and 58°, respectively, in contradiction to the theory. Thus, a

simple counter-rotation theory is insufficient to describe the orientational relationship between the g tensor and imidazole ligands in *Dv*MF cytochrome c_3.

We prefer a simpler explanation for the relationship. By looking at the angles in a different way, it can be said that the g_y axis co-rotates with the imidazole plane of the sixth ligand for heme 1 (41° and 50°), heme 2 (−55° and −63°), and heme 3 (−25° and −19°) and the g_x axis co-rotates with that for heme 4 (56° and 52°). Taking the maximal error in the angles (9.9°) into account, all relationships can be reasonably classified to the co-rotation. Using an average angle of two imidazoles does not change the situation for heme 1, heme 3, and heme 4. So, we are not claiming that the sixth ligand is the determinant. Although the counter-rotation gives a better agreement for heme 1, there is no reason to discriminate this heme from the others. The reason of the exchange of the axes in heme 4 is not clear. Anyway, the magnetic property of heme 4 seems different from those of the other hemes. Our conclusion is different from that of Turner et al.[17] This disagreement might come from the difference between the g tensor and the magnetic susceptibility. The change of the crystal structure depending on temperature is unlikely, because the crystal structures determined at 11 °C and 100 K were found identical expect for a couple of side chains.[25,45] This problem is left open for future investigation.

This research was partly supported by a Grant-in-Aid for Scientific Research on Priority Area from the Ministry of Education, Culture, Sports, Science and Technology and by a grant from CREST (Core Research for Evolutional Science and Technology), Japan.

References

1 J. M. Odom and H. D. Peck, Jr., *FEMS Microbiol. Lett.*, **12**, 47 (1981).
2 K. Ozawa, T. Meikari, K. Motohashi, M. Yoshida, and H. Akutsu, *J. Bacteriol.*, **182**, 2200 (2000).
3 K. Niki, Y. Kobayashi, and H. Matsuda, *J. Electroanal. Chem.*, **178**, 333 (1984).
4 K. Kimura, Y. Nakayama, T. Yagi, and H. Inokuchi, *J. Chem. Phys.*, **70**, 3317 (1979).
5 Y. Nakamura, K. Kimura, H. Inokuchi, and T. Yagi, *Chem. Phys. Lett.*, **73**, 31 (1980).
6 K. Fan, H. Akutsu, Y. Kyougoku, and K. Niki, *Biochemistry*, **29**, 2257 (1990).
7 J.-S. Park, T. Ohmura, K. Kano, T. Sagara, K. Niki, Y. Kyogoku, and H. Akutsu, *Biochim. Biophys. Acta*, **1293**, 45 (1996).
8 D. L. Turner, C. A. Salgueiro, T. Catarino, J. LeGall, and A. V. Xavier, *Biochim. Biophys. Acta*, **1187**, 232 (1994).
9 D. L. Turner, C. A. Salgueiro, T. Catarino, J. LeGall, and A. V. Xavier, *Eur. J. Biochem.*, **241**, 723 (1996).
10 M. Coletta, T. Catarino, J. LeGall, and A. V. Xavier, *Eur. J. Biochem.*, **202**, 1101 (1991).
11 R. O. Louro, T. Catarino, D. L. Turner, M. A. Picarra-Pereira, I. Pacheco, J. LeGall, and A. V. Xavier, *Biochemistry*, **37**, 15808 (1998).
12 J. P. Gayda, T. Yagi, H. Benosman, and P. Bertrand, *FEBS Lett.*, **217**, 57 (1987).
13 H. Benosman, M. Asso, P. Bertrand, T. Yagi, and J. P. Gayda, *Eur. J. Biochem.*, **182**, 51 (1989).
14 J. P. Gayda, H. Benosman, P. Bertrand, C. More, and M. Asso, *Eur. J. Biochem.*, **177**, 199 (1988).
15 I. Moura, M. Teixeira, B. H. Huynh, J. LeGall, and J. J. Moura, *Eur. J. Biochem.*, **176**, 365 (1988).
16 B. Guigliarelli, P. Bertrand, C. More, R. Haser, and J. P. Gayda, *J. Mol. Biol.*, **216**, 161 (1990).
17 D. L. Turner, L. Brennan, A. C. Messias, M. L. Teodoro, and A. V. Xavier, *Eur. Biophys. J.*, **29**, 104 (2000).
18 N. V. Shokhirev and F. A. Walker, *J. Am. Chem. Soc.*, **120**, 981 (1998).
19 A. M. Raitsimring and F. A. Walker, *J. Am. Chem. Soc.*, **120**, 991 (1998).
20 D. Inniss, S. M. Soltis, and C. E. Strouse, *J. Am. Chem. Soc.*, **110**, 5644 (1988).
21 H. Hori, *Biochim. Biophys. Acta*, **251**, 227 (1971).
22 A. L. Tsai and G. Palmer, *Biochim. Biophys. Acta*, **681**, 484 (1982).
23 F. A. Walker, B. H. Huynh, W. R. Scheidt, and S. R. Osvath, *J. Am. Chem. Soc.*, **108**, 5288 (1986).
24 O. Q. Munro, J. A. Serth-Guzzo, I. Turowska-Tyrk, K. Mohanrao, T. Kh. Shokhireva, F. A. Walker, P. G. Debrunner, and W. R. Scheidt, *J. Am. Chem. Soc.*, **121**, 11144 (1999).
25 Y. Higuchi, M. Kusunoki, Y. Matuura, N. Yasuoka, and M. Kakudo, *J. Mol. Biol.*, **172**, 109 (1984).
26 E. Harada, Y. Fukuoka, T. Ohmura, A. Fukunishi, G. Kawai, T. Fujiwara, and H. Akutsu, *J. Mol. Biol.*, **319**, 767 (2002).
27 J. R. Postgate, "The Sulphate-Reducing Bacteria," 2nd ed, Cambridge University Press, Cambridge, UK (1984), pp. 30–42.
28 J.-S. Park, K. Kano, Y. Morimoto, Y. Higuchi, N. Yasuoka, and M. Ogata, *J. Biomol. NMR*, **1**, 271 (1991).
29 D. S. Schonland, *Proc. Phys. Soc., London*, **73**, 788 (1959).
30 C. A. Salgueiro, D. L. Turner, J. LeGall, and A. V. Xavier, *J. Biol. Inorg. Chem.*, **2**, 343 (1997).
31 C. P. Taylor, *Biochim. Biophys. Acta*, **491**, 137 (1977).
32 J. G. Ma, J. Zhang, R. Franco, S. L. Jia, I. Moura, J. J. Moura, P. M. Kroneck, and J. A. Shelnutt, *Biochemistry*, **37**, 12431 (1998).
33 F. A. Walker and U. Simonis, *J. Am. Chem. Soc.*, **113**, 8652 (1991).
34 M. Nakamura and N. Nakamura, *Chem. Lett.*, **1991**, 1885.
35 T. Saitoh, T. Ikeue, Y. Ohgo, and M. Nakamura, *Tetrahedron*, **53**, 12487 (1997).
36 M. Nakamura, T. Ikeue, H. Fujii, and T. Yoshimura, *J. Am. Chem. Soc.*, **119**, 6284 (1997).
37 T. Ikeue, Y. Ohgo, T. Saitoh, M. Nakamura, H. Fujii, and M. Yokoyama, *J. Am. Chem. Soc.*, **122**, 4068 (2000).
38 T. Ikeue, Y. Ohgo, T. Saitoh, T. Yamaguchi, and M. Nakamura, *Inorg. Chem.*, **40**, 3423 (2001).
39 J. Peisach, W. E. Blumberg, and A. Adler, *Ann. N.Y. Acad. Sci.*, **206**, 310 (1973).
40 M. Czjzek, F. Payan, F. Guerkespquin, M. Bruschi, and R. Haser, *J. Mol. Biol.*, **243**, 653 (1994).
41 R. Pierattelli, L. Banci, and D. L. Turner, *J. Biol. Inorg. Chem.*, **1**, 320 (1996).
42 L. Banci, R. Pierattelli, and D. L. Turner, *Eur. J. Biochem.*, **232**, 522 (1995).
43 D. L. Turner, *Eur. J. Biochem.*, **227**, 829 (1995).
44 I. Bertini, C. Luchinat, G. Parigi, and F. A. Walker, *J. Biol. Inorg. Chem.*, **4**, 515 (1999).
45 K. Ozawa, Y. Takayama, F, Yasukawa, T. Ohmura, M. A. Cusanovich, Y. Tomimoto, H. Ogata, Y. Higuchi, and H. Akutsu, *Biophys. J.*, **85**, 3367 (2003).